Dentomaxillofacial Radiology (2005) 34, 205–211

http://dmfr.birjournals.org

RESEARCH

Software for automated application of a reference-based method for *a posteriori* determination of the effective radiographic imaging geometry

RKW Schulze*,[1], O Weinheimer[2], DD Brüllmann[3], F Röder[1], B d'Hoedt[1] and E Schoemer[2]

[1]Department of Oral Surgery (and Oral Radiology), Johannes Gutenberg-University, Mainz, Germany; [2]Institute for Computer Science, Johannes Gutenberg-University, Mainz, Germany; [3]Department of Operative Dentistry, Johannes Gutenberg-University, Mainz, Germany

Objectives: Presentation and validation of software developed for automated and accurate application of a reference-based algorithm (reference sphere method: RSM) inferring the effective imaging geometry from quantitative radiographic image analysis.

Methods: The software uses modern pattern recognition and computer vision algorithms adapted for the particular application of automated detection of the reference sphere shadows (ellipses) with subpixel accuracy. It applies the RSM algorithm to the shadows detected, thereby providing three-dimensional Cartesian coordinates of the spheres. If the three sphere centres do not lie on one line, they uniquely determine the imaging geometry. Accuracy of the computed coordinates is investigated in a set of 28 charge-coupled device (CCD)-based radiographs of two human mandible segments produced on an optical bench. Each specimen contained three reference spheres (two different radii $r_1 = 1.5$ mm, $r_2 = 2.5$ mm). True sphere coordinates were assessed with a manually operated calliper. Software accuracy was investigated for a weighted and unweighted algebraic ellipse-fitting algorithm.

Results: The critical depth- (z-) coordinates revealed mean absolute errors ranging between 1.1 ± 0.7 mm (unweighted version; $r = 2.5$ mm) and 1.4 ± 1.4 mm (weighted version, $r = 2.5$ mm), corresponding to mean relative errors between 5% and 6%. Outliers resulted from complete circular dense structure superimposition and one obviously deformed reference sphere.

Conclusions: The software provides information fundamentally important for the image formation and geometric image registration, which is a crucial step for three-dimensional reconstruction from ≥ 2 two-dimensional views.

Dentomaxillofacial Radiology (2005) **34,** 205–211. doi: 10.1259/dmfr/56357032

Keywords: radiography, dental, digital; technology, radiologic; image processing, computer-assisted

Introduction

It is well known that the projection (imaging) geometry, *i.e.* the spatial relation between X-ray source, object and imaging plane relative to one another, is the fundamental basis for radiographic image formation. Theoretical work concerning its standardization in intraoral radiography was published in 1969.[1] However, foreshortening or elongation due to an oblique position of a given object under examination in the projection geometry still is a well-known problem in two-dimensional (2D) dental intraoral radiography.[2–4] Due to the anatomical obstacle of the hard palate, radiographs in the upper jaw are particularly prone to such distortions, which yield considerable errors when linear measurements are performed.[5] Unfortunately, in general, the projection geometry is at best known partly, *e.g.* in applying a holding device-based paralleling technique, where the focal spot is fixed relative to the image receptor. This technique resembles the well-known C-arm design in medical radiography. Generalizing a 2D method for calculating the angular relationship between the object and a given receptor axis,[6] we have

---

*Correspondence to: Dr Ralf Schulze, Poliklinik für Zahnärztliche Chirurgie, Augustusplatz 2, 55131 Mainz, Germany; E-mail: rschulze@mail.uni-mainz.de
Received 10 May 2004; revised 24 January 2005; accepted 24 March 2005

developed a reference-based algorithm (reference sphere method: RSM), which allows for *a posteriori* calculation of the effective imaging geometry by means of quantitative image analysis.[7] In its most general form, the algorithm only requires the temporary fixation of three radiopaque ball bearings (spheres) of known diameter to a rigid object under study, and the *a priori* knowledge of the source-to-receptor distance. Primarily, RSM geometrically determines the 3D positions of the spheres, thereby providing three known "object"-points in space. In addition, RSM enables simple reconstruction of the point of incidence of the normal dropped from the focal spot onto the image-plane. This is equivalent to constituting five (three rotations of the image-plane plus two translations of the focal spot relative to this plane) out of six possible degrees of freedom between the two components, only leaving the distance between them remaining unknown.[7] If it is to be used in a clinical environment, the RSM algorithm requires software implementation to enable easy, accurate and fast application.

The aim of this report is to introduce a software solution for the automated application of RSM. More specifically, the software was designed to fulfil the following requirements: (i) automated detection and classification of the 2D reference sphere shadows in real world radiographs containing structural noise; and (ii) automated RSM-based calculation of the 3D coordinates of each reference sphere within the effective projection geometry.

This article will describe a software solution developed according to these specifications. In addition, it will present results from an *ex vivo* validation experiment designed for the assessment of accuracy of the software with respect to its fundamental target: the localization of the reference spheres in 3D from quantitative analysis of their 2D radiographic shadows.

Material and methods

RSM-algorithm

A detailed description of the RSM algorithm may be obtained from prior work of the authors.[7] In brief, the algorithm exploits the 2D information inherent in the shadows of radiopaque reference spheres to localize their centres of gravity in three dimensions with respect to a given Cartesian coordinate system (Figure 1). Here, the depth- (z-) axis is aligned with the normal (in general, the central X-ray) dropped from the focal spot onto the x–y-receptor-plane and intersects the latter in the origin (0,0,0). It should be noted that, in this paper and the current software version, the conventional notation and coordinate system used is contrary to the original publication,[7] where the depth axis had been labelled as x-axis. RSM makes use of the fact that the projection of a sphere onto a flat imaging-(receptor-)plane will generally be an ellipse.[8] Only if the central X-ray passes though the sphere centre and intersects the imaging plane at right angles will the shadow truly be a circular disc. The algorithm makes use of the known geometrical correspondence between the projected major axis of the 2D ellipse and the 3D coordinates of the X-ray tangent points at the 3D sphere. In perspective geometry, the connecting line between the tangent points is mapped to the major ellipse axis. From this known correspondence and the 2D location of the radiographic sphere shadow the 3D position of the sphere's centre of mass is computed.[7] In addition, the fact that the line extended through each major elliptical axis contains the point of incidence (0,0,0) of the central X-ray on the image receptor may be used for reconstruction of this important reference point.[7] If the source-to-receptor distance is known *a priori*, in the absence of noise, the 3D coordinates of each sphere's centre of mass within the imaging geometry can be determined exactly. These points may be labelled as "extrinsic object points". In case of a rigid object under study with three spheres attached to it in arbitrary, but non-collinear positions, it is well known that the knowledge of the 3D coordinates of three non-collinear points in space entirely constitutes the rigid coordinate transformation occurring between different views of one scenery (see, for instance Betke et al[9]). In addition, RSM enables simple *a posteriori* reconstruction of the point of incidence of the central X-ray on the receptor-plane. This combination of geometric information, without any further restrictions, is equivalent to knowing the entire imaging geometry. The latter provides the fundamental basis for 3D reconstruction from ≥ 2 2D views.[10–12]

RSM-software

The software is developed with Borland C++ Builder 6 (Borland GmbH, Langen, Germany), using the raw image files as basic input data after conversion into 16 bit Tiff-files by a tool (XSensTest, Version 1.0) provided by the manufacturer of the radiographic unit (Sirona Dental Systems GmbH, Bensheim, Germany). The data are subsequently converted into a 8 bit DICOM-File-Format. Pixels with grey values above a certain threshold are recorded in a detection matrix of image size, since it is reasonable to assume that the 2D images of the reference spheres are represented by grey values among the highest within the radiograph. Holes in the segmentation are closed by geodetic closing.[13] In cases of partial occlusion by dense structures, a circle-based Hough Transform[14] is used to reconstruct the shadow, *i.e.* its geometric centre. We set aside a computationally more costly five-dimensional ellipse-detecting Hough Transform. Instead, the boundary refinement and ellipse fitting algorithms specified below are applied on the truncated non-occluded arc of the ellipse. By means of region growing the pixels in the detection matrix are clustered into continuous objects.[15] Clusters exceeding a threshold area (10×10 pixel) are further tested for roundness R,[16] with

$$R = \frac{4F}{\pi d_{\max}^2} \in [0, 1] \tag{1}$$

where F denotes the area covered by the pixels and $d_{\max}$ the maximum distance within the object as assessed through its centre of gravity C. The roundest objects are defined as sphere shadows and will be further referred to as ellipses. All other objects are deleted from the detection matrix.

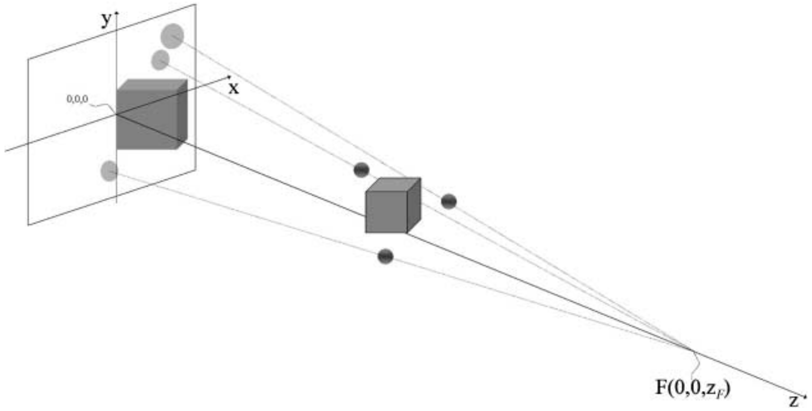

Figure 1 Projective imaging geometry as effective in typical radiographic images exposed in a C-arm or holding device-based radiographic technique. We define a Cartesian coordinate system, with the z-axis aligned with the central X-ray (normal dropped from the source point $F(0,0,z_F)$), which intersects the flat $x-y$-detector plane in the origin (0,0,0). An arbitrary but non-collinear triplet of reference spheres of known dimensions is temporarily attached to a rigid object under investigation (here: cube). Using the projection lines, RSM infers the true 3D location of each sphere from its 2D shadow, thereby constituting the object's six possible degrees (three translational and three rotational) of freedom

Since the RSM algorithm is fundamentally based on the quantitative assessment of the major elliptical axes, accurate boundary identification at each ellipse is of crucial importance. Therefore, using a commercial charge-coupled device (CCD)-receptor (Full Size; Sirona Dental Systems GmbH, Bensheim, Germany), a series of exposures of a naked steel sphere (radius 2.50 mm) glued onto a low-absorbing acrylic stick was obtained on an optical bench at nine distances (42 mm to 122 mm, at steps of 10 mm) from the receptor. From the very beginning, we used this series for software calibration. A boundary refinement algorithm was designed for the purpose of subpixel-accurate border detection. 256 radial scanlines reaching from C towards the periphery of each ellipse (and actually exceeding it) are constructed and their density profiles are recorded. Neglecting local minima, the contrast between the sphere image and the background is investigated and the line revealing maximum contrast (defined as 100%, Figure 2) among all three sphere shadows is recorded. The global minimum grey value is defined as g_B, whereas local background minima as measured along each individual scanline are denoted by g_S. The rationale for this approach is that an ellipse will be most accurately detected if it is completely surrounded by only minimally absorbing structures (*e.g.* air). The transformation of an ideal rectangular input signal due to the point spread effect mathematically is a convolution of this signal with the (mostly unknown) point spread function (PSF) of the imaging system.[17] From this observation and under the assumption of an unknown PSF, we deduced a linear approximation to find an accurate boundary definition (Figure 3). In the subpixel domain, the signal may be modelled as a continuous signal composed of 2D-Gaussians, the latter representing the approximation of the point spread effect. Based on the well known "full width at half maximum" technique we developed an algorithm referred to as "Full width at x[%] of the maximum". Here, x is determined by:

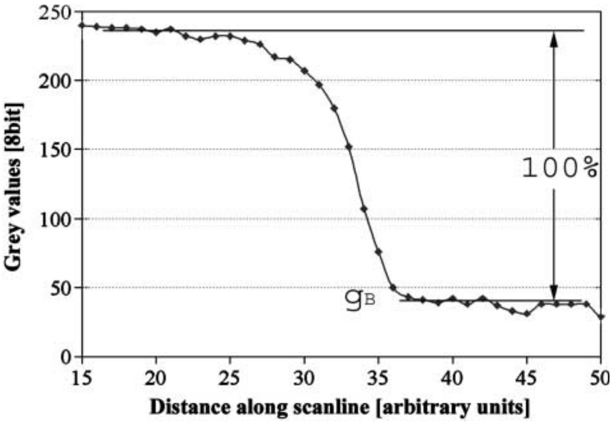

Figure 2 Grey-scale profile as assessed along one scanline in the ellipse boundary refinement process. The particular scanline represents that line revealing the highest global contrast (100%), among all scanlines of all three sphere shadows. g_B is defined as globally minimum grey value in the periphery of any of the three sphere 2D shadows. It is used for a global calibration of the boundary refinement algorithm

$$x = \mathrm{Max}\left(g_{\min}, g_{\max} - 0.03\left(\frac{g_S}{g_B} - 1\right)\right) \tag{2}$$

where, considering the point spread effect, $g_{\min}$ and $g_{\max}$ refer to lower (10%) and upper (40%) bounds, where the true border of the ellipse is to be expected according to empirical results. The factor 0.03 was also determined empirically from the calibration series. The desired grey value g_E defining the boundary point along each scanline is obtained from:

$$g_E = g_S + x(g_C - g_S) \tag{3}$$

with g_C representing the grey value at the centre of gravity C. All values are computed in the subpixel domain. The so-computed boundary points are used in an algebraic ellipse fitting algorithm,[18] where the "algebraic distance" $F(\mathbf{a}, \mathbf{x_i})$ between a general conic section (including ellipses)

$$F(\mathbf{a}, \mathbf{x}) = \mathbf{a}\,\mathbf{x} = ax^2 + bxy + cy^2 + dx + ey + f = 0 \tag{4}$$

with $\mathbf{a} = [a\ b\ c\ d\ e\ f]^T$ and $\mathbf{x} = [x^2\ xy\ y^2\ x\ y\ 1]$, and a data point (x_i, y_i) is to be minimized by minimizing the sum of

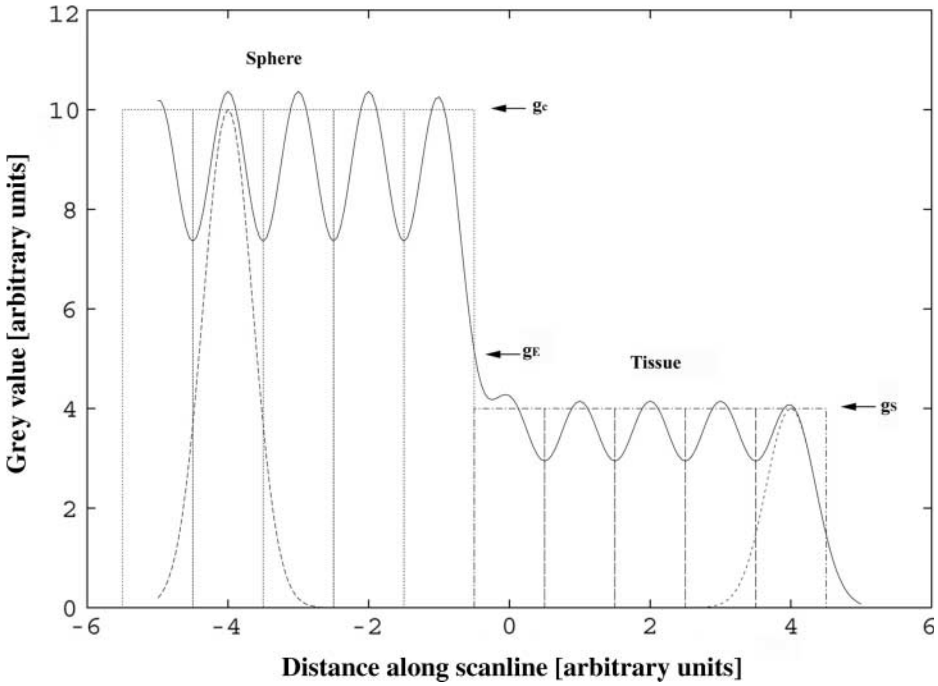

Figure 3 Modelling of the point spread effect with Gaussian curves superimposed over the ideal, rectangular response function. The transition between the high grey values representing the shadow of the sphere (left side) and the lower values produced by a superimposed, less dense structure (right side of curve) is the area, where the "true" ellipse boundary has to be identified with subpixel accuracy. This is currently done by a linear interpolation based on empirically determined data, where the intersection of the Gaussian with the ideal response function is assumed to represent the "true" ellipse border. The corresponding grey value g_E is computed from the global minimum g_B and linear interpolation (Equations (2) and (3))

squared algebraic distances

$$D(\mathbf{a}) = \sum_{i=1}^{N} F(\mathbf{a}, \mathbf{x_i})^2 \tag{5}$$

of the curve on $N = 256$ data points. In addition, due to the above described rational, a linear weighting factor

$$w_i = \frac{g_B}{g_S} \tag{6}$$

is introduced, assigning the "pre-estimated boundary point" (x_i, y_i) along each scanline a weight proportional to the local gradient. w_i enters Equation (5) as follows:

$$D(\mathbf{a}) = \sum_{i=1}^{N} (w_i\, F(\mathbf{a}, \mathbf{x_i}))^2 \tag{7}$$

After computing the best-fitting ellipses for the unweighted (Equation (5)) as well as for the weighted (Equation (7)) case, their major axes in combination with their 2D locations are recorded with subpixel accuracy. These input data enter the RSM algorithm implemented in the software. To minimize the propagation of numerical rounding errors, the software uses 64 bit-floating values (doubles). In the final step, the software computes the 3D coordinates of each sphere's centre of mass $M_k(x_{M_k}, y_{M_k}, z_{M_k})$, $k \in [1, 2, 3]$.

Experimental validation

Since the software must be robust enough to handle real-world radiographs, we decided to use dry human mandible sections obtained from the Department of Anatomy. Two segments were each equipped with three non-collinear reference spheres (section No.1: radius 1.50 mm; section No.2: radius 2.50 mm) placed in an area sufficiently small and close to the objects of interest (teeth) to be imaged on the dental CCD-receptor specified above. Exposures were obtained on an optical bench (Figure 4) providing a perpendicular incidence of the central X-ray in the centre (origin of the coordinate system, Figure 1) of the CCD-receptor described before. Due to the marginal elliptical distortion on the small area intraoral sensor and to avoid additional input error, we decided not to use the *a posteriori* reconstruction of the coordinate system's origin. Pixel spacing was 0.039 mm. Exposures in six arbitrarily selected

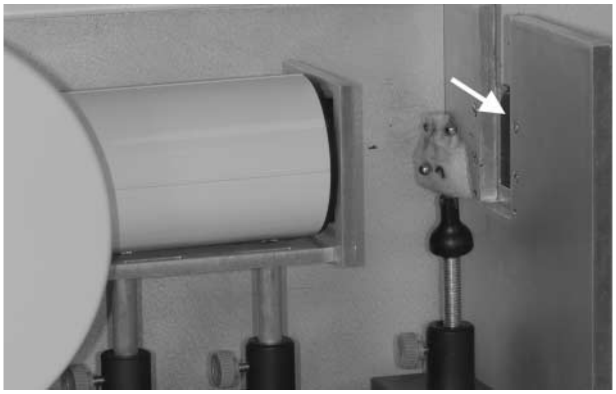

Figure 4 Experimental set-up on an optical bench, showing the specimen with the reference spheres attached in arbitrary, but non-collinear positions. Arrow indicates the position of the charge-coupled device (CCD)-sensor

spatial positions were obtained per specimen, with each position exposed in two relevant exposure times (0.04–0.08 s) determined after subjective contrast evaluation with respect to visual image quality. From previous experiments we had learned that scatter equivalents did not influence depth accuracy significantly, thus no scatter phantom was applied. To avoid additional errors, we only included sphere shadows which were not partly occluded by equally dense objects (amalgam or gold restorations). Eighteen reference sphere positions (3 spheres times 6 positions) were obtained per segment, and a total of 24 radiographs (12 per specimen times 2 specimens) entered the evaluation. "True" coordinates c_t were assessed by means of a calliper as accurately as possible. Due to the construction of the optical bench and the human phantom, only the depth-(z-)coordinates could be measured with tolerable accuracy of roughly ± 0.5 to ± 0.75 [mm]. Depth coordinates, however, are the fundamental output of the RSM algorithm, since x- and y-coordinates are linearly correlated with them. Due to beam convergence towards the source, errors in the latter coordinates necessarily need to be significantly smaller than depth errors. Hence, we only included registration of the z-coordinates in our experimental evaluation of the software.

Absolute errors e_a were computed, *i.e.* absolute differences between "true" (c_t) and computed coordinates (c_o) of each of the three spheres in each position. In addition, relative errors e_r were calculated in terms of:

$$e_r = \frac{c_t - c_o}{c_t} 100\ [\%] \qquad (8)$$

Possible interactions between e_{a_z} as dependent variable and sphere size and absolute depth as factors were investigated in a one-way analysis of variance (ANOVA). In case of a detected dependency, the Spearman Correlation Coefficient R was also computed (SPSS for Windows 11.0; SPSS Inc., Chicago, IL). Errors between the weighted and unweighted algorithm were compared by means of the paired Wilcoxon test.

Results

Depth accuracy for the calibration series revealed errors entirely below 1 mm (mean -0.08 mm; range -0.56–0.39 mm) for all object-to-receptor distances. Within the human mandible series, we observed an underestimation of true depth, with an average e_{a_z} of 1.4 ± 1.1 mm for $r = 1.5$ mm for both the unweighted and weighted algorithm. For $r = 2.5$ mm, the average e_{a_z} was 1.4 ± 1.4 mm as computed with the weighted version versus 1.1 ± 0.7 mm with the unweighted version (Table 1; Figure 5). The paired Wilcoxon test did not reveal a significant difference between both versions ($P = 0.240$). Outliers ($e_{a_z} > 3$ mm) are rare for the unweighted version ($N_{\text{unweighted}} = 4$), but more frequent for the weighted ellipse fitting ($N_{\text{weighted}} = 7$; Figure 5). Although not explicitly statistically evaluated, outliers were mainly found in ellipses circularly superimposed by dense structures such as bone. It is noteworthy that three out of the four outliers produced by the unweighted algorithm are related to one single reference sphere, which, compared with the specifications from the manufacturer, revealed a slightly larger, but inconsistent radius (≈ 1.6 mm). Obviously this sphere had been deformed in the production process. Although we calculated the values with the corrected radius (1.60 mm), however, the deformation yielded the reported remaining depth error. The corresponding average relative depth error ranged between 5% and 6% (Table 1). Absolute errors in depth were significantly dependent on sphere diameter (ANOVA; unweighted: $P \leq 0.001$; weighted: $P = 0.005$), however, the Spearman correlation was very weak (unweighted: $R = 0.034$; weighted:

Table 1 Descriptive statistics of absolute (lines 3 to 6) and relative (lines 9 to 12) errors for the critical depth-(z-)coordinate. Absolute errors were defined as the difference in millimetres between true and calculated values. Relative errors represent the ratio between absolute error and true coordinates (in percent). Within each group, errors are given for the unweighted and the weighted version of the algebraic ellipse fitting process

		Absolute error [mm]		
Radius [mm]		*Mean ± SD*	*Median*	*Range*
1.5	Weighted	1.4 ± 1.1	0.9	0.11; 4.01
	Unweighted	1.4 ± 1.1	1.1	0.02; 4.14
2.5	Weighted	1.4 ± 1.4	1.1	0.04; 6.14
	Unweighted	1.1 ± 0.7	0.9	0.01; 3.27
		Relative error [%]		
		Mean ± SD	Median	Range
1.5	Weighted	5.5 ± 4.4	3.6	0.6; 17.8
	Unweighted	5.5 ± 4.5	4.9	0.2; 19.2
2.5	Weighted	5.5 ± 4.6	4.4	0.06; 17.5
	Unweighted	4.8 ± 3.7	4.1	0.04; 16.8

SD, standard deviation

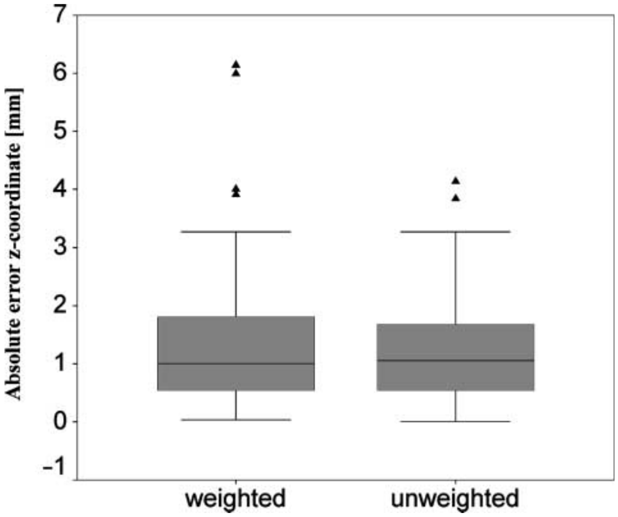

Figure 5 Boxplots of absolute errors in the critical depth-(z-) coordinate separated for the weighted (left) and unweighted (right) version of the algorithm. The boxes contain the data between the 25% and 75% percentile, with the median indicated by a bold horizontal line. The whiskers include all values lying not further than three box lengths outside the box. Outliers are indicated by small triangles. While the vast majority of errors for both approaches ranged between 0.5 mm and 1.8 mm, there were more outliers observed for the weighted version (see also Table 1)

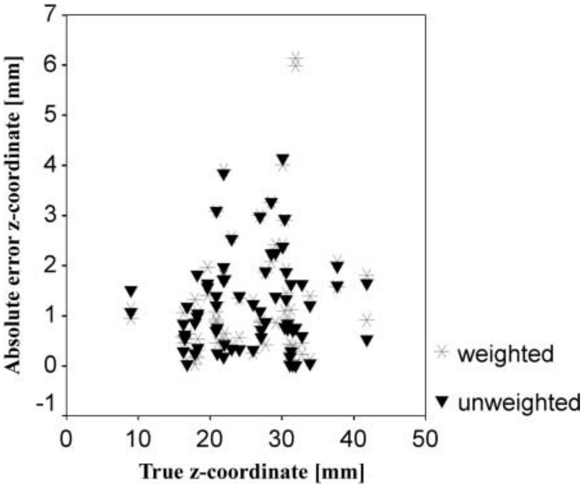

Figure 6 Modified Bland-Altman plot, where accuracy (y-axis) in terms of absolute differences between calculated and true z-coordinates is plotted against the true z-coordinates (x-axis) for the unweighted and weighted algorithm. An absolute error of "0" indicates best possible agreement. The plot shows no trend towards increasing depth coordinates, indicating neither a loss nor a gain in accuracy

$P = 0.131$). No significant correlation was found between actual ("true") depth and the respective depth error (unweighted: $P = 0.029$; weighted: $P = 0.160$). This finding is also supported by the modified Bland Altman plot (Figure 6),[19] which shows neither a positive nor a negative trend towards increasing depth values.

Discussion

The reference sphere method RSM provides depth coordinates of reference objects (metallic spheres) of known size. These coordinates, however are not computed from simply relating 2D magnification to 3D dimension by application of the rule of proportion. Instead, using *a priori* knowledge about the geometrical relationship between a computable 3D distance within the reference sphere and the 2D major axis of the ellipse cast by the sphere, it provides mathematically precise 3D coordinates of the sphere's centre of mass.[7] Of course, in reality the input data are corrupted by noise, thus the output coordinates will contain error. In the absence of error, by calculating three non-collinear points (the centre points of three spheres temporarily attached to a rigid object under study), RSM constitutes all six remaining degrees of freedom (three translations plus three rotations) of an object exposed within a C-arm-like imaging geometry.[7] Since a dental holding device resembles a C-arm technique by fixing the source relative to the sensor in a reproducible and measurable position, the entire imaging geometry in such an environment is constituted. Although not done here to reduce the overall error due to a small ratio between major and minor ellipse axis in small-scale intraoral radiography, another very important property of RSM is to identify the point where the normal dropped from the focal spot intersects the imaging plane (origin of the coordinate system). The knowledge of this reference point reduces the six possible degrees of freedom between image receptor and focal spot (neglecting rotations of the latter being non-relevant due to its point shape) to only one: the (z-) distance between these two components. If not only relative positions are to be computed, the algorithm requires the *a priori* knowledge of exactly this distance. We believe that this restriction is relatively unproblematic, since holding devices which represent the golden standard for intraoral radiography are commonly used already. The required distance may be easily obtained once from the dimensions of the holding device and the tube. From theoretical considerations we also know that practically relevant errors within this distance have only minor influence on depth accuracy.[7] In larger scale extraoral applications, the origin of the coordinate system may be easily reconstructed by identifying the 2D image point of closest approach between the lines extended through the three major ellipse axes.

The complete knowledge of the imaging geometry is particularly important for 3D reconstruction from a set of 2D radiographic images of a given situation.[10,11] Hence, RSM can be used to register several radiographic images with respect to the geometric transformation having occurred between the images. Our software was designed to provide a fully automated application of the RSM algorithm on digital radiographs. More specifically, it analyses the image automatically, detects the reference sphere shadows and performs the quantitative RSM analysis to produce 3D Cartesian coordinates for each reference sphere. From a physical point of view, the depth- (z-) coordinate should be the least accurate, since it is calculated from fitting the 3D spheres into the tangent projection-lines indicated by the endpoints of the 2D major ellipse axis.[7] Hence, the major axes have to be identified as accurately as possible. By considering the point spread effect and global contrast maxima for calibration of the ellipses' gradient profiles, the implemented boundary definition algorithm interpolates the demanded distance also in the presence of a small local gradient. In doing so, initial estimates are obtained indicating the "true" boundary of the elliptic shadow. The algebraic ellipse fit, either weighted or unweighted, fits an ellipse in a least square sense into these data points. Both the initial estimations as well as the final ellipse fit proceed in the subpixel domain, to produce a best possible estimation of the shadow's 2D dimension. Our experimental results still reveal a slight underestimation of the ellipse's major axis, resulting in an underestimation of true depth. The automatic detection procedure erroneously assigns pixels to neighbouring structures or background, although they are actually belonging to the sphere's shadow. This is probably due to different sorts of noise and the non-linear degrading of grey values towards the shadow's boundary. As anticipated from theoretical considerations, this effect is particularly pronounced when a sphere shadow is completely superimposed by radio-dense structures occluding the ellipse boundaries. We neglect the erroneous results caused by the slightly deformed sphere. Although a global calibration is implemented, it should be noted that typical dental images would rarely provide a location where a highest possible gradient, *i.e.* only air superimposition, will be found. Obviously, the simple linear weighting function currently implemented is unable to sufficiently compensate for this local effect. One solution may be a weighting function, compensating for a low overall local contrast (*i.e.* the gradient along all 256 scanlines) in one shadow. Another more specific approach would be to measure the system's PSF and deconvolute the image with that function. Altogether, a significant depth-error reduction is noticeable, when the software results are compared with the values based on the manual, cursor-based assessment procedure reported in Schulze et al.[7] Interestingly, the anticipated error reduction resulting from increased reference sphere radius was only very small in our experiment, most probably due to the computation in the subpixel domain. This finding makes the method more applicable in small size intraoral radiography, where, compared with large area medical radiographs, the occlusion caused by the spheres is a relevant drawback of the method. Although the software is able to reconstruct the shadow using a circle-based Hough Transform, we did not experimentally evaluate the error induced by metallic partial superimposition over sphere shadows. The subsequent boundary refinement and algebraic fitting procedure will be based on a truncated arc of the ellipse, since the boundary refinement will be erroneous within the entire superimposed shadow area. It is to be expected that the fit based on such truncated data will produce a decreased ellipse dimension,[18] *i.e.* further underestimation of true depth.

Errors in the critical z-coordinate will propagate into x- and y-coordinates; however, due to the beam convergence towards the source, errors in the latter coordinates must be significantly smaller than the depth errors themselves.

To further improve registration accuracy we are currently implementing a secondary approach making use of the invariant provided by the triangle between the 3D sphere centres. Yet, the theoretical assumption that this additional information increasing with the number of views should reduce the remaining error, has to be proved experimentally. The research will now proceed to the reconstruction of 3D structure from at least two 2D radiographs, which, in theory, is a straightforward task once the geometric transformation between the underlying radiographs is known.[10–12] However, due to its extremely under-determined nature, additional *a priori* information has to be included, *e.g.* using the Bayesian statistics as described in Robinson et al, Kolehmainen et al and Siltanen et al.[11,20,21]

In conclusion, the software introduced here may be used for geometric radiographic image registration. Since the data provided are already 3D, the accuracy of the software should be reasonable for such purposes. Knowing the geometric transformation having occurred between several 2D views of one 3D scenery enables straight forward reconstruction of the 3D information content inherent in the 2D views. The reconstruction problem is currently addressed in this ongoing research project.

Acknowledgments

The work reported here is part of an ongoing research project funded by the German Research Foundation (DFG), project SCHU 1496/1-1 and SCHU 1496/1-2. We explicitly acknowledge the Department of Anatomy for providing us with the human mandible segments.

References

1. van Aken J. Optimum conditions for intraoral roentgenograms. *Oral Surg Oral Med Oral Pathol* 1969; **27:** 475–491.
2. Payne AG, Solomons YF, Lownie JF. Standardization of radiographs for mandibular implant-supported overdentures: review and innovation. *Clin Oral Implants Res* 1999; **10:** 307–319.
3. Sewerin IP. Errors in radiographic assessment of marginal bone height around osseointegrated implants. *Scand J Dent Res* 1990; **98:** 428–433.
4. Webber RL, Ruttimann UE, Groenhuis RA. Computer correction of projective distortions in dental radiographs. *J Dent Res* 1984; **63:** 1032–1036.
5. Schulze R, d'Hoedt B. Mathematical analysis of projection errors in "paralleling technique" with respect to implant geometry. *Clin Oral Implants Res* 2001; **12:** 364–371.
6. Schulze R, d'Hoedt B. A method to calculate angular disparities between object and receptor in "paralleling technique". *Dentomaxillofac Radiol* 2002; **31:** 32–38.
7. Schulze RK, Brüllmann DD, Röder F, d'Hoedt B. Determination of projection geometry from quantitative assessment of the distortion of spherical references in single-view projection radiography. *Med Phys* 2004; **31:** 2849–2854.
8. Hilbert D, Cohn-Vossen S. *Geometry and the imagination*, 2 edn. New York, NY: Chelsea Publishing Co., 1991.
9. Betke M, Hong H, Thomas D, Prince C, Ko JP. Landmark detection in the chest and registration of lung surfaces with an application to nodule registration. *Med Image Anal* 2003; **7:** 265–281.
10. Cheriet F, Meunier J. Self-calibration of a biplane x-ray imaging system for an optimal three dimensional reconstruction. *Comput Med Imaging Graph* 1999; **23:** 133–141.
11. Robinson SB, Hemler PF, Webber RL. A geometric problem in medical imaging. *Proc SPIE* 2000; **4121:** 208–217.
12. Metz CE, Fencil LE. Determination of three-dimensional structure in biplane radiography without prior knowledge of the relationship between the two views: theory. *Med Phys* 1989; **16:** 45–51.
13. Soille P. *Morphologische Bildverarbeitung: Grundlagen, Methoden, Anwendungen*. Berlin, Heidelberg, New York: Springer Verlag; 1998.
14. Hough PVC. Methods and means for recognizing complex patterns. USA patent n.3,069,654. 1962.
15. Lehmann TM, Oberschelp W, Pelikan E, Repges R. *Bildverarbeitung für die Medizin*. Berlin: Springer Verlag; 1997.
16. Handels H. *Medizinische Bildverarbeitung*. Stuttgart, Leipzig: Teubner Verlag; 2000.
17. Rossmann K. Point spread-function, line spread-function, and modulation transfer function. Tools for the study of imaging systems. *Radiology* 1969; **93:** 257–272.
18. Fitzgibbon A, Pilu M, Fisher R. Direct least square fitting of ellipses. *IEEE Trans Pattern Anal Machine Intell* 1999; **21:** 476–480.
19. Bland JM, Altman DG. Statistical methods for assessing agreement between two methods of clinical measurement. *Lancet* 1986; **1:** 307–310.
20. Kolehmainen V, Siltanen S, Järvenpäa S, Kaipio JP, Koistinen P, Lassas M, et al. Statistical inversion for medical x-ray tomography with few radiographs: II. Application to dental radiology. *Phys Med Biol* 2003; **48:** 1465–1490.
21. Siltanen S, Kolehmainen V, Järvenpäa S, Kaipio JP, Koistinen P, Lassas M, et al. Statistical inversion for medical x-ray tomography with few radiographs: I. General theory. *Phys Med Biol* 2003; **48:** 1437–1463.